Statistical Downscaling of Seasonal Wave Forecasts

P. Camus[1], S. Herrera[2], J.M. Gutiérrez[3], I. J. Losada[1]

[1]Environmental Hydraulics Institute "IHCantabria", Universidad de Cantabria, Spain

[2]Meteorology Group, Dpto. de Matemática Aplicada y Ciencias de la Computación, Universidad de Cantabria, Santander 39005, Spain

[3]Meteorology Group, Instituto de Física de Cantabria (CSIC-UC), Santander 39005, Spain

Corresponding author: Paula Camus (camusp@unican.es)

Key words:

Seasonal forecast; statistical downscaling; significant wave height; Western Pacific; Atlantic Ocean

Abstract

Despite the potential applicability of seasonal forecasting for decision making in construction, maintenance and operations of coastal and offshore infrastructures, tailored climate services have yet to be developed in the marine sector. In this work, we explore the potential of a state-of-the-art seasonal forecast systems to predict wave conditions, particularly significant wave height. Since this information is not directly provided by models, a statistical downscaling method is applied to infer significant wave height based on model outputs such as sea level pressure, which drive waves over large wave generation areas beyond the target location over time. This method may be beneficial for seasonal forecasting since skill from wide generation areas can be propagated to wave conditions in (distant and smaller) target regions. We consider seasonal predictions with a one-month lead time of the CFSv2 hindcast in two regions: the Western Pacific around Indonesia during the June-July-August (JJA) season and the North Atlantic Ocean during the January-February-March (JFM) season. In the former case, skillful predictions are found, which are higher during decay years after ENSO warm phases when a negative anomaly of the significant wave height is expected. In contrast, statistical downscaling in the North Atlantic Ocean cannot add value to the signal given by the predictor, which is also very weak.

1 Introduction

Seasonal forecasting has great potential for use in a wide range of planning and maintenance activities that are strongly dependent on seasonal to interannual climate variations. Global predictions at this time scale are routinely produced by only a few centers around the world using coupled ocean-atmosphere models, due to both the specialized knowledge and the computational resources required. Although seasonal predictability over most extratropical regions is still limited (Doblas-Reyes et al., 2013), more skillful predictions are expected in the near future due to the recent advances in new potential predictability sources (Dunstone et al., 2016, Clark et al., 2017). The recent adoption of climate services (Hewitt et al., 2013, Bruno Soares et al., 2018) has boosted the development of tailored products for decision making in different sectors (see, e.g., the COPERNICUS Sectoral Information System over Europe, https://climate.copernicus.eu/sectoral-information-system). Sectoral applications of seasonal forecasting are now being established in several sectors, such as agriculture, energy and water management (Bruno Soares et al., 2018). Other recently discovered applications are emerging, including early-warning systems for heat wave-related mortality (Lowe et al., 2016) and fire danger (Bedia et al., 2018). However, climate services have yet to be developed in other areas, such as the marine sector, which has several potential applications based on seasonal wave predictions (significant wave height and others) in planning for the construction, maintenance and operations of coastal (e.g., ports) and offshore (e.g., wind farms) infrastructures.

Two recent studies investigated the skills of global models in predicting significant wave height, and these studies focused on tropical regions (West Pacific and Indian Oceans) where moderate-to-high skill is expected (Lopez and Kirtman, 2016 and Shukla and Kinter, 2016). These studies showed that El Niño-Southern Oscillation (ENSO) has a nonlinear influence on a smaller than normal wave height during summers after the ENSO warm phase. This wave height variability is due to a reduced atmospheric synoptic activity associated with a strengthening of the West Pacific subtropical high, which is also related to an ENSO decay (Yun et al., 2015). One source of seasonal forecasts skill in the tropics is the finding that ENSO teleconnections are generally robust to internal atmospheric variability in this region (Brands, 2017). The ENSO also dominates the wind variabilities in the equatorial region and swell wave variabilities in the Southern Hemisphere of the Pacific Ocean (Stopa and Cheung, 2014).

In the North Atlantic region, the wintertime mean wind and wave conditions are largely driven by atmospheric circulation patterns such as the North Atlantic Oscillation (NAO) and the East Atlantic (EA) and Scandinavian (SCAND) patterns (Trigo et al., 2008). The moderate skill of global models in predicting these large-scale patterns has motivated the development of alternative empirical techniques, which rely on the lagged relationships between slowly varying components of the climate system and the predictand of interest. Colman et al. (2011) predicted winter ocean wave heights for the preceding month of May in the North Sea based on North Atlantic Sea surface temperatures (SSTs). As an alternative to this classic predictor, the October Eurasian snow cover increase was recently found to highly correlate with the DJF mean Arctic Oscillation (AO) (Cohen and Jones 2011). Based on this hypothesis, Brands (2014) proposed a statistical technique for forecasting the DJF mean wind and wave conditions in the North Atlantic based on the Eurasian snow cover increase in October. Castelle et al. (2017) recently defined a new climate index called the Western Europe Pressure Anomaly (WEPA) based on the sea level pressure gradient between the Valentia (Ireland) and Santa Cruz de Tenerife (Canary Islands) stations, and the WEPA explains the greater winter wave height variability along the Atlantic coast of Europe better than other leading atmospheric modes.

The potential value added by using dynamical and statistical downscaling methods to improve the skill of global forecasts over particular regions of interest was recently explored in a number of intercomparison studies. Manzanas et al. (2018a) assessed the value added by performing dynamic and statistical downscaling for seasonal temperature predictions in Europe. Nikulin et al. (2018) performed a similar study for East African precipitation. The added value of dynamic downscaling was shown to be limited, whereas statistical downscaling methods (building on the link between large-scale atmospheric predictors and the local predictand of interest) could yield significant skill improvements in those cases where the large-scale variables used as predictors are better predicted by the global model than the local variable of interest (see Manzanas et al. 2018b). These methods are also suitable for predicting variables that are not directly provided by the model but that can be statistically connected to some model variables.

The potential predictability of the wave climate is largely linked to the predictability of the wind or sea level pressure fields, which is a common predictor used in statistical downscaling approaches (Wang et al., 2014). On the other hand, the global wave field is found to be dominated by swell, even along extratropical storm areas, where the relative weight of the wind-sea part of the wave spectra is highest (Semedo et al., 2011). Swells are generated remotely and are not directly coupled to the local wind field. Therefore, local target waves are strongly connected to the large-scale predictors of global model simulations. In principle, statistical downscaling methods could take advantage of atmospheric teleconnections by extending the predictor region well beyond the target region (Manzanas et al., 2018b). Therefore, there is the potential to improve the wave seasonal forecast skill as a result of aggregating predictability of distant wave generation areas. In this paper, we explore this possibility by adapting a statistical downscaling method for waves recently introduced by Camus et al. (2017) and by assessing the method's added value for seasonal forecasting using the retrospective seasonal forecasts provided by the publicly available CFSv2 seasonal hindcast (Saha et al., 2011). We focus on two regions: 1) the Western Pacific around Indonesia during the June-August (JJA) season because of the wave climate forecast skill associated with the El Niño-Southern Oscillation (ENSO) variability, which was previously analyzed in Lopez and Kirtman (2016) and Shukla and Kinter (2016), and 2) the North Atlantic Ocean during the January-March (JFM) season, which is the period with the highest interannual variability mainly associated with NAO pattern (Woolf and Challenor, 2002). The experiments are limited to the predictions corresponding to lead month 1 (May/December initializations) for the JJA/JFM season in the Western Pacific and North Atlantic.

This paper is organized as follows. In Section 2, the data used for both the predictand and predictors and the wave climate characterization of the two regions being studied are introduced. The statistical downscaling methodology applied in this study and the validation of the statistical model are described in Section 3. The forecast quality verification is presented in Section 4. Finally, the relevant conclusions of this study are summarized in Section 5.

2 Data

Historical predictand (waves) and predictor (sea level pressure) information is required to calibrate the (perfect prog) statistical downscaling model. In addition, a retrospective forecast dataset is used to verify the performance of the seasonal forecasts. The historical wave database is also used to assess the forecast quality of the downscaled wave heights. Historical information from the El Niño and NAO indices is also used to analyze the connection of these indices to the summer or winter wave conditions in the Western Pacific and North Atlantic, respectively.

2.1 Historical data

2.1.1 Historical Wave Data

The wave hindcast GOW2 was developed by Perez et al. (2017) and provides historical wave data (i.e., significant wave height, H_s, peak wave period, T_p, and mean wave direction, θ) with an hourly resolution and spatial resolutions of 0.5° at the global scale and 0.25° along the worldwide continental shelf coast from 1979 to present. This hindcast uses the wave model WaveWatch III (version 4.18, Tolman, 2014) with the parameterization TEST451 (Ardhuin et al., 2010) in a multigrid configuration, which is driven by the wind and ice coverage fields interpolated from historical CFSR and CFSv2 data, respectively (Saha et al., 2014).

Figure 1 shows the mean and 95th percentiles of the JJA H_s in the Western Pacific (upper panels) and the JFM H_s in the North Atlantic (lower panels). In the Western Pacific, differences in the spatial patterns of various statistics (mean, and 95th and 99th percentiles) reflect the differences in wave generation processes. Most extreme events are concentrated around the Philippine Sea, which matches the high percentile plots obtained by Stopa et al. (2012) and Timmermans et al. (2017) and the seasonal distribution of the 20-year return level quantile (Izaguirre et al., 2011). Mean conditions reflect only the wave generation due to local winds (Indonesia) or distant extratropical storms (eastern Australia and eastern Asia), with the highest mean wave height of approximately 2.0 m in eastern Australia and 1.6 m in the Northwest Pacific Ocean. The extreme wave conditions concentrated in the Philippine Sea area can be explained by the larger frequency and intensity of tropical cyclones (TCs) in this region, reaching values of approximately 4.0 m and 6.0-7.0 m for the 95th and 99th percentiles (not shown), respectively. The tracks of the extratropical storms in the North Atlantic determined the spatial patterns of the waves. The patterns of the two wave statistics (mean and 95th percentile, 99th percentile is not shown) are similar in the North Atlantic (see also Stopa et al., 2012), with the highest waves at approximately 40°N and 65°N and values reaching 5.0 and 9.0 m for the mean and 95th percentile conditions, respectively (11.0 m for the 99th percentile).

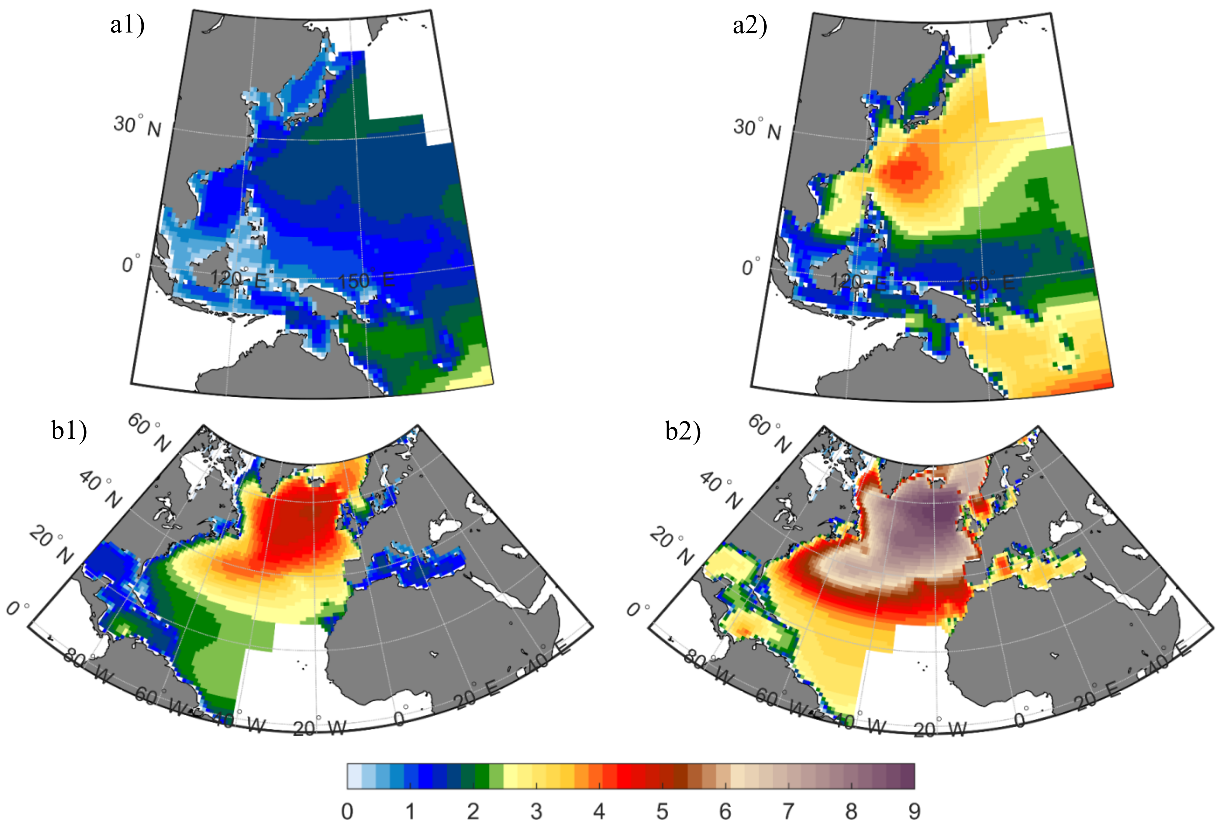

Figure 1. JJA Hs (m) in the Western Pacific (a) and JFM Hs in the North Atlantic (b): 1) Mean; 2) 95th percentile as computed from the GOW2 dataset over the 1979-2016 period.

2.1.2 Historical Atmospheric Data

Historical sea level pressure (SLP) is obtained from the Climate Forecast System Reanalysis (CFSR and CFSRv2, Saha et al., 2014), which is the reanalysis corresponding to the seasonal forecasting systems that are considered in this study (see Sec. 2.2). The temporal coverage spans from 1979 to present with an hourly temporal resolution and 0.5° spatial resolution**.**

2.1.3 Climate Indices

The Oceanic Niño Index (ONI), defined as the 3-month running mean of ERSST.v5 SST anomalies in the Niño 3.4 region (5°N-5°S, 120°-170°W), which is centered on 30-year base periods that are updated every 5 years (Huang et al. 2017), is used as a measure of the ENSO in this work. The Climate Prediction Center (CPC), part of the National Ocean and Atmospheric Administration of the United States (NOAA), has adopted a new updating strategy for the base period to define El Niño and La Niña episodes and remove warming trends in the Niño-3.4 region (https://origin.cpc.ncep.noaa.gov/products/analysis_monitoring/ensostuff/ONI_change.shtml). Warm (El Niño) and cold (La Niña) periods are identified based on a threshold of +/- 0.5°C for the ONI and when the threshold is met for a minimum of 5 consecutive overlapping seasons. As a result, El Niño events for the 1982-2010 period are 1982, 1986, 1987, 1991, 1994, 1997, 2002, 2006 and 2009. The ENSO usually begins to increase in spring, peaks during boreal winter and decreases afterward, becoming much weaker in the following summer. For this reason, the NDF (November-December-January) ONI is used to analyze the summer wave climate variability in the Western Pacific. The correlation of the wave climate in JJA in the Western Pacific with the NDJ ONI for the 1979-2016 period is shown in the upper panels of Figure 2. The spatial patterns of the correlation with the wave statistics parameters (mean and 95th and 99th percentiles; only the first two are shown) are quite similar. A high positive correlation is found in nearly the whole area, while a significant negative correlation is found around New Guinea.

The North Atlantic Oscillation (NAO) is traditionally defined as the normalized pressure difference between two stations: one is in the Azores and the other is in Iceland. An extended version has been used in this study based on one station in the SW part of the Iberian Peninsula (Hurrell, 1995), Gibraltar, and the other station is in SW Iceland (Jones et al., 1997), which are derived for the winter half of the year and calculated by the Climatic Research Unit (CRU) of the University of East Anglia.The correlation between the JFM Hs and NAO Index is shown in the lower panels of Figure 2. A positive correlation at the highest latitudes and a negative correlation at the lowest latitudes can be observed, which is consistent with prior studies (Dodet et al., 2010, Bromirski and Cayan, 2015). Note than the correlation in some grid nodes over the Gulf of Saint Lawrence and the western part of Labrador Sea is not represented because the ocean is sometimes frozen during winter. The developed downscaling technique is not suitable for areas with sea ice cover as the predictor definition only considers the sea level pressure fields and none information about ice is introduced. Moreover, seasonal sea ice cover predictions are not available from the CFSv2 retrospective database.

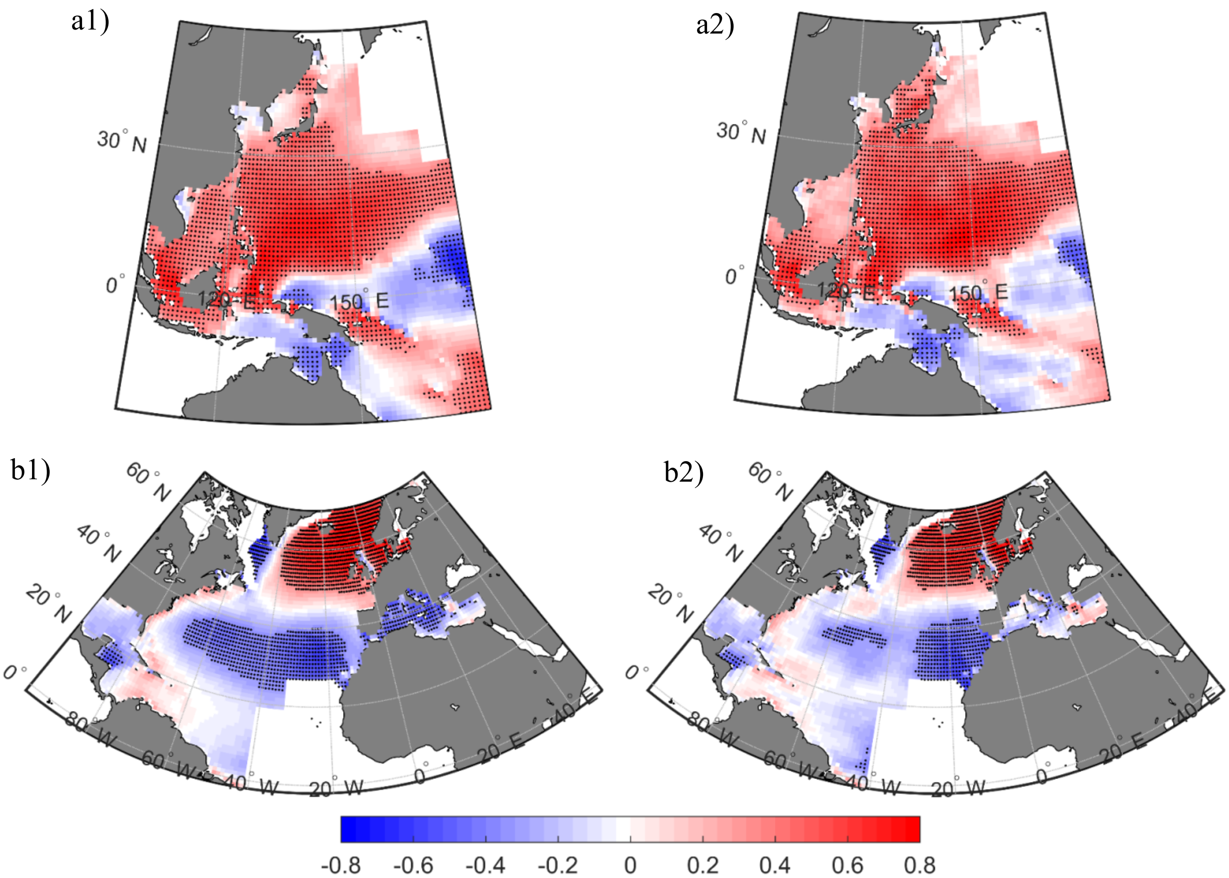

Figure 2. Correlation between the Western Pacific JJA H_s and NDJ ONI: a1) Mean and a2) 95th percentile of the JJA H_s. Correlation between the North Atlantic JFM H_s and NAO Index: b1) Mean and b2) 95th percentile of JFM H_s. Stippling represents areas where the correlation is statistically significant at 5% level.

2.2 Seasonal forecast data (hindcast)

The NCEP CFSv2 seasonal forecasting system is used in this study to evaluate wave climate predictability at the seasonal scale. The 28-year (1982-2009) ensemble retrospective forecast, known as the qua, dataset from CFSv2 with 24 members is provided by NCEP (Saha et al., 2011). The CFSv2 used in the reforecast consists of the NCEP Global Forecast System at T126 (~0.937° resolution), the Geophysical Fluid Dynamics Laboratory Modular Ocean Model version 4.0 at 0.25-0.5° grid spacing coupled with a two-layer sea ice model, and the four-layer NOAH land surface model.

The NCEP-CFSv2 forecast database is consistent with the reanalysis atmospheric database (NCEP Global Forecast System) used to calibrate the statistical downscaling model. This forcing is used to generate the GOW2 database and is publicly available.

This information is retrieved from the ECOMS User Data Gateway (ECOMS-UDG), which is developed by the Meteorology Group of the Universidad de Cantabria (Cofiño et al., 2018), in the framework of the European Climate Observations, Modelling and Services initiative (ECOMS) projects. ECOMS coordinates the activities of three on-going European projects (EUPORIAS, SPECS and NACLIM), with a focus on seasonal to decadal predictions. The ECOMS-UDG facilitates harmonized multimodel seasonal forecast data. This information can be obtained directly from the data providers, but this activity is error-prone and time-consuming because the resulting formats, temporal aggregations and vocabularies may not be homogeneous across datasets.

Historical reanalysis and retrospective CFSR SLP data are converted to a common 2.0ºx2.0º latitude-longitude grid. Daily predictor fields are standardized to avoid biased results due to differences in climate model climatology and variability. In the case of GCMs, standardization is applied using the simulated seasonal climatological mean and seasonal standard deviation of the retrospective seasonal forecast database for the historical period covering 1982-2009.

3. Seasonal Forecast Downscaling Methodology

3.1. Statistical downscaling approach

This study was built on the statistical downscaling (SD) method developed by Camus et al. (2017) based on weather types (WTs) under the so-called perfect prog approach, adapting the method to the particularities of seasonal forecasting. This downscaling approach relies on a relationship established between observed large-scale predictors and observed local-scale predictands. The predictor defined by the daily sea level pressure (SLP) fields from the reanalysis CFSR atmospheric database over the local wave (predictand) generation area is classified into a reduced number of WTs (100 in this work). The GOW2 dataset is used as predictand data. A regression guided classification is applied to a combination of the weighted predictor and predictand estimations from a regression model, which links the SLP fields with the local marine climate. First, the statistical relationship is established by identifying hourly sea state parameters at each location of interest in each daily predictor field within the corresponding cluster. Then, the empirical probability distribution of each sea state parameter (e.g., significant wave height) associated with each WT is calculated. Finally, the complete distribution of this variable for a particular time period can be estimated as the probability sum of each WT during that period multiplied by the corresponding empirical distribution. As a result, different statistics (e.g., mean, 95th percentile) can be derived from the estimated distribution.

Daily SLP and daily squared SLP gradients (SLPG) are usually taken as atmospheric variables to define the wave predictor, since SLPG fields are proven to improve the statistical relationship with waves (Wang et al., 2014). A performance verification of the retrospective SLP and SLPG seasonal forecasts was carried out (not shown) before establishing the final version of the predictor for the statistical downscaling model at the seasonal scale. A low predictability of SLPG is found, which could deteriorate the forecast quality of the seasonal wave climate. Therefore, this variable is eliminated as a predictor from the statistical downscaling model.

The predictor spatial domain for each area of study is based on the wave generation patterns obtained in Camus et al. (2017). The domain for the Western Pacific Ocean covers a great part of the Pacific Ocean from 120°E to 150°W and from 60°N to 54°S. The predictor domain for the North Atlantic extends from 64°W to 16°E and from 0°N to 76°N. The predictor is defined as the leading principal components (PCs), which explain 95% of the entire predictor variance of the m-daily mean SLP, with m=7 days for the Western Pacific and m=3 days for the North Atlantic. These values were obtained on the same day and the previous m-1 days as the SLP average throughout the historical time period. PCs are calculated for the seasonal forecasts by projecting the corresponding standardized fields onto the empirical orthogonal functions obtained from the reanalysis, which are used for the calibration of the method.

Following Manzanas (2016), who obtained a more skillful statistical downscaling model for seasonal precipitation forecasting using season-specific data in the model calibration, a particular regression-guided classification is performed at every wave GOW2 grid node at a 1.0^0 resolution, considering the multivariate wave conditions (H_s, T_p, θ) independently in each season. One-hundred SLP field WTs are obtained for every GOW2 grid node. The seasonal empirical distribution of hourly significant wave height associated with each WT at every grid node of the GOW2 wave database is calculated.

The most similar semiguided WT is identified for each m-daily mean SLP field from the hindcast database CFSRv2-NCEP to calculate the probability of WTs and infer the seasonal empirical distribution of the significant wave height at each grid node during the target season. The seasonal predictions of the mean and the 95th and 99th percentiles of the significant wave height are obtained to assess the seasonal forecast quality.

3.2 Statistical model cross-validation

The SD model performance must be evaluated to obtain an upper bound for the model's generalization capability when applied to new predictor data (large-scale variables from GCM). The most popular approach used in climate applications to validate an SD model for the historical period independent of the training period involves data splitting. In particular, in this work, a k-fold cross-validation, which uses multiple calibration/validation period combinations to produce a more rigorous validation (see, e.g., Kohavi, 1995 for a general discussion or Gutiérrez et al. 2013 for an application in statistical downscaling), was performed considering $k=5$ to obtain a calibration/test period covering 80%/20% of the full period for each fold (Casanueva, 2016). As a result, five independent and stratified folds (7/8 years each) covering the full period have been defined by selecting 1 per 5 years, i.e., the first fold would be formed in years 1979, 1984, 1989, 1994, 1998, 2004, 2009 and 2014. Using this option, the same distributions/climatologies are sampled for all folds, and each fold covers a more representative range of years (Gutiérrez et al., 2013).

The estimates from the statistical downscaling model are compared against the parameters obtained from the observations (GOW wave data) at a monthly scale during the JJA season in the Western Pacific and during the JFM season in the North Atlantic. The monthly mean and 95th and 99th percentiles of H_s are validated using the corresponding sea-state parameter distribution associated with each WT during the calibration period of each k=5 test subset. The Pearson correlation coefficient, normalized root mean square error (NRMSE), which is defined as the root mean square error divided by the mean observed value (expressed in %), and bias are computed for each H_s parameter using the entire 1979-2015 period by joining the test subsets into a single prediction.

3.2.1 Western Pacific

The validation scores are shown in Figure 3 for the mean and 95th percentile of the significant wave height (mean in the left column, 95th percentile in the right column). The skill of the SD model is considerably high but worsens for higher H_s percentiles. The correlation coefficients are approximately 0.8-0.95 for the mean Hs in nearly the whole area, except in the most sheltered part, such as the coast of the China Sea and north of New Guinea, where the value decreases to 0.5. The correlation decreases for extreme wave heights, and there are restricted areas with coefficients of approximately 0.8. Regarding the NRMSE, the values increase from approximately 10% for the mean Hs to 20% for the 95th percentile and between 30% and 50% for the 99th percentile (not shown) in the area with the highest extreme waves generated by TCs. The bias (not shown) is nearly negligible for the mean significant wave height and small for the extreme percentiles.

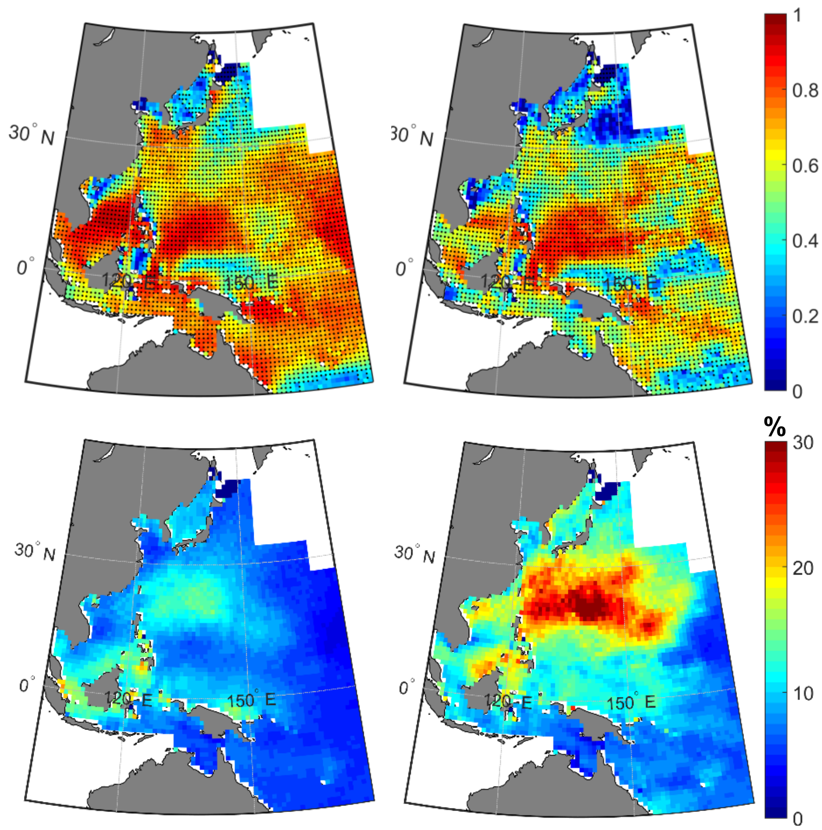

Figure 3. Validation of the SD model during the JJA season for the monthly mean (left column) and 95th percentile (right column) of H_s in the Western Pacific Ocean by means of the correlation coefficient (upper row) and normalized root mean square error (lower row). Stippling represents areas where the correlation is statistically significant at 5% level.

3.2.2 North Atlantic

Figure 4 shows the correlation coefficient and NRMSE, which are computed for the two statistics of JFM H_s (in columns) for the entire 1979-2015 period using a 5-fold cross-validation. The skill of the SD model is considerably high for the mean conditions but worsens as the H_s percentile increases. The correlation coefficients are approximately 0.9-0.95 for nearly the entire area (decreasing to values of approximately 0.5 in the western part of the Mediterranean Sea and Caribbean Sea). Regarding the NRMSE, the values increase from approximately 5% for the mean Hs to 10% for the 99th percentile. The bias (not shown) does not suggest a clear trend to over or underestimate Hs.

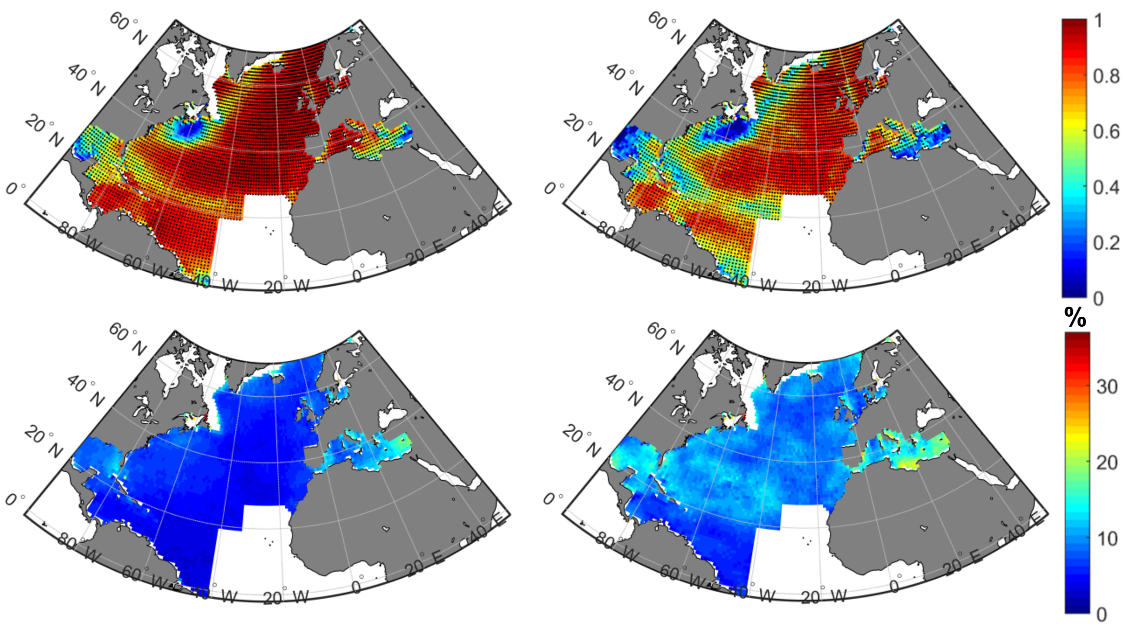

Figure 4. Validation of the SD model in the JFM season for the monthly mean (left column) and 95th percentile (right column) of H_s in the North Atlantic by means of the correlation coefficient (upper panel) and normalized root square mean error (lower panel). Stippling represents areas where the correlation is statistically significant at 5% level.

4. Seasonal Forecast quality

4.1. Verification metrics

An assessment of quality based on past performance is required to give value to the prediction itself (Doblas-Reyes et al., 2013). A range of additional verification measures are applied to provide a complete description of different quality aspects relevant to users (Jolliffe and Stephenson, 2003). In this work, the correlation coefficient and the bias are used for a deterministic verification (ensemble mean). The Ranked Probability Score (RPS), the Ranked

Probability Skill Score (RPSS) and the Relative Operating Characteristic Skill Score (ROCSS) are used for probabilistic verification.

The bias is a metric of the mean forecast deviation from the observations. On the other hand, the correlation coefficient measures the temporal correspondence between the forecast and observational reference, which is insensitive to linear transformations of the data and thus complementary to the bias. In this study, an ensemble mean interannual series of the mean and 95th and 99th percentiles of the seasonal Hs forecasts is calculated from the predicted time series for each of the 24 CFSv2 members at each grid GOW2 node of the two study areas.

In addition, a tercile-based approach is used for the probabilistic verification of the prediction quality (Frías et al. 2010). The interannual series of seasonal predictions of the mean and 95th and 99th percentiles of the significant wave height are classified into three categories (above, near or below-normal), according to the respective climatological terciles. The categories were calculated for each particular grid node and each particular member (24 in the case of NCEP CFSv2). A probabilistic forecast is computed annually (1982-2009) by considering the number of members falling within each category (a dataset of 28 probabilistic forecasts for the below, near and above-normal categories).

The ranked probability score (RPS) is a measure of forecast quality based on the squared forecast probability error, which is cumulative across the three forecast categories from lowest to highest (3 in a tercile-based system). The error (see equation 1) is the squared difference between the cumulative forecast probability up to category icat ($Pcumfct_{icat}$), where *icat* is the category number (1 for below normal, 2 for near normal, and 3 for above normal) and the corresponding cumulative observed "probability" (*Pcumobs*), where 1 is assigned to the observed category and 0 is assigned to the other categories. Note that a higher RPS indicates a greater forecast probability error. RPS is defined as follows:

$$\boldsymbol{RPS = \frac{1}{ncat-1}\sum_{icat=1}^{ncat}\left(Pcumfct_{icat} - Pcumobs_{icat}\right)^2} \quad (1)$$

where *ncat* is the number of categories (3 in a tercile-based approach).

The ranked probability skill score (RPSS) is based on a comparison of the ranked probability score (RPS) for an actual set of forecasts (RPS_{fct}), where the RPS corresponds to constant climatology (0.333/0.333/0.333) forecasts (RPS_{clim}). A positive RPSS implies that the RPS is lower for the forecasts than it is for the climatology forecasts. Higher scores indicate forecasts with higher skill levels.

$$\mathbf{RPSS = 1 - \frac{RPS_{fct}}{RPS_{clim}}} \quad (2)$$

The relative operating characteristic (ROC) curve measures forecast quality in terms of discrimination ability. The ROC is constructed by plotting the hit rate against the false alarm rate using a set of increasing probability thresholds (e.g., 0.05, 015, 0.25), which define the probability bins. A hit implies an accurate forecast (true positive) of a particular event, such as below normal wave severity, while a false alarm implies a false positive for the nonoccurrence of such an event. The ROC curve involves subdividing the probabilistic forecast dataset (i.e., 28 seasonal predictions for the 1982-2009 period) into separate probabilistic bins (defined by the probability thresholds). The points on the ROC curve are initially created using only those predictions within the bin with highest forecast probabilities and sequentially adding predictions in successively decreasing forecast probabilities. A hit implies an accurate forecast (true positive) of a particular event, such as below normal wave severity, while a false alarm implies a false positive for the nonoccurrence of such an event. A ROC curve is calculated individually for each forecast tercile.

The ROC skill score (ROCSS, the area under the ROC curves) characterizes the system's ability to correctly anticipate the occurrence or nonoccurrence of predefined events. An ROCSS above 0.5 reflects a positive discrimination skill, and 1.0 represents a perfect forecast system. A value of zero indicates no skill with respect to a climatological prediction. This skill measure is independent of the model bias.

4.2. Forecast verification

4.2.1 Western Pacific

The correlation coefficient is a simple metric that is used to assess the ability of the downscaled 24-member ensemble JJA wave height to reproduce the observed interannual variability of the significant wave height over the 28 year period (1982-2009). The correlation coefficient is shown in the upper panels of Figure 5 for the mean and 95th percentile significant wave height. In general, the correlation coefficients are found to be significant (values of approximately 0.4-0.6). The TC frequency is related to the ENSO, and therefore, the JJA interannual variability in terms of higher wave heights, which increases the predictability of these extremes. The JJA climatology bias of the mean and 95th percentile wave height is depicted in the lower panels of Figure 5. The bias is negligible for the mean H_s, slightly negative (5%) for the 95th percentile, and mostly limited to the TC region.

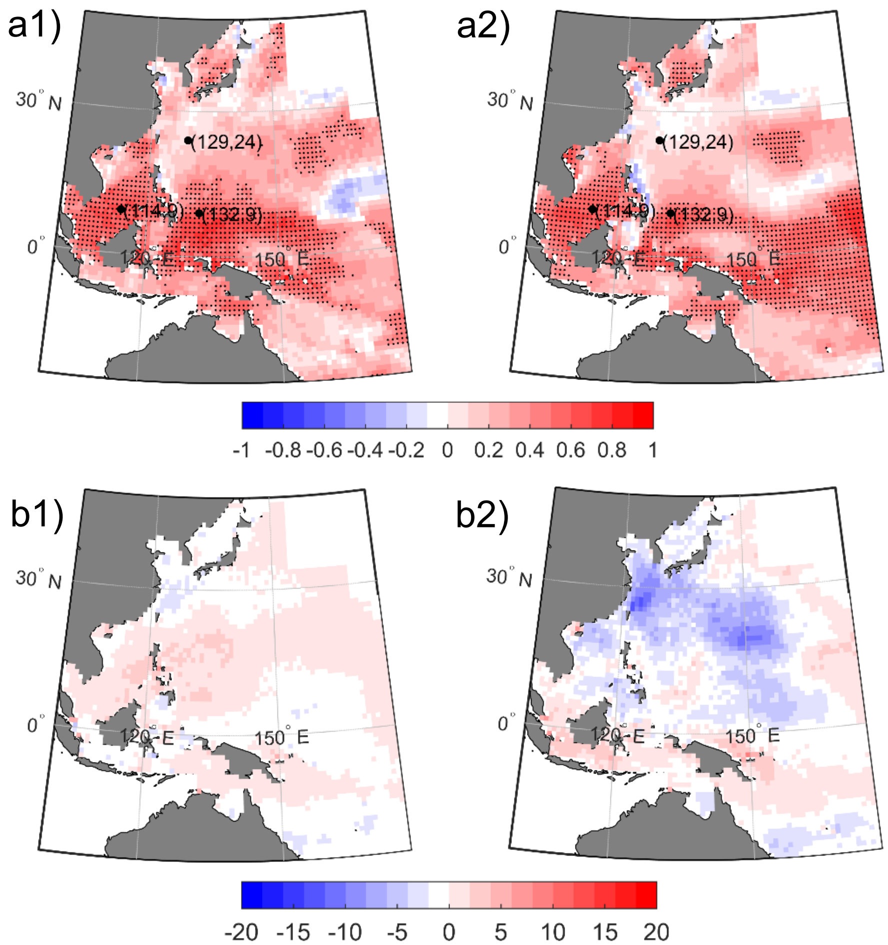

Figure 5. Upper panels: Correlation coefficient between the observed and predicted JJA Hs in the Western Pacific Ocean: a1) mean and a2) 95th percentile. Lower panels: Bias (in %) of the predicted JJA significant wave height climatology: b1) mean and b2) 95th percentile. Stippling represents areas where the correlation is statistically significant at 5% level.

As an illustrative example of the tercile-based probabilistic validation approach, Figure 6 shows the 1979-2010 standardized historical time series of the 95th percentile of the JJA H_s observations and NDJ ONI with correlation coefficients and tercile validation plots for several grid points with different wave climate and forecast skills (see Frías et al., 2018 for a detailed description of the tercile plot). The standardized H_s time series provides information about the high interannual variability in the seasonal wave climate in this area. Higher waves are observed during strong warm ENSO phases (high values of the NDJ ONI) and a wave height decrease is seen the following summer season. The tercile plot represents the interannual (1982-2009) time series of probabilistic predictions from the 24 members of the CFSR-v2 seasonal database as the number of members falling in each tercile, which are arranged by rows with the probability represented in grayscale, and the binary occurrence/nonoccurrence calculated from the observations is shown for the three terciles (marked by a dot inside the box).

The best relationship with ONI is found at location [Lon=132.0°; Lat=9.0°] (panel a), with the smallest waves are usually found in the summer following El Niño years (1982, 1986, 1987, 1991, 1994, 1997, 2002, 2006 and 2009 with the highest NDJ ONI values marked in pink). The forecast resolution generally increases during El Niño years (see lower tercile with the highest forecast probabilities and the observed occurrence marked with a green dot in panel 2 of Figure 6), especially after the strongest El Niño events (1987 and 1997). Most of the years with high negative wave anomalies (1983, 1988, 1995, 1998, 2007, and 2010) are connected to the QB-type ENSO cases. These types of ENSO events are characterized by a rapid change from El Niño in the preceding winter to La Niña in the following summer or SST differences that are greater than 2.0º C between the preceding winter and ensuing summer (i.e., 1982/1983). The QB-type ENSO is also related to the strengthening of the subtropical highs located in the western North Pacific (Yun et al., 2014). These results suggest that the predictability signal in this region and season is linked to this variability mode. Years with observed upper terciles (i.e., 1997, 2002, 2006 and 2009, marked with blue dots) are well predicted, indicating a certain predictability of the SLP fields transferred to downscaled wave heights. These years with waves within the above-normal category coincide with El Niño years. The TC genesis tends to have longer lifetimes, be more intense and form in greater numbers over the central Pacific region during warm ENSO phases (Camargo et al., 2007), which begins to increase during the spring of those years. In addition, this higher TC activity is reflected in higher waves, mainly in the area of the Philippine Sea, where the wave severity is associated with TCs.

The correlation with the Niño 3.4 index is smaller for location [Lon=114.0°; Lat=9.0°] (see panel b). However, the relationship between the high index values and small waves (below tercile) can still be detected, with significant forecasting skill after El Niño years (1982, 1988, 1995 and 1998). Regarding the upper tercile (above-normal), the forecast predictions reached values of approximately 0.5-0.6, especially during the 1999-2002 period. In the case of location [Lon=129.0°; Lat=9.0°], shown in panel c of Figure 6, almost no skill (ROCSS is near zero) is found. This grid is located in an area with high differences between spatial patterns of the mean and high percentiles because of high extreme waves resulting from TC generation. Therefore, the lack of forecast quality at this location may be related to errors in GCMs when simulating TCs. Despite the generally nonsignificant skill throughout the historical years (1982-2009), the observed below-normal terciles after the strongest QB-type ENSO cases are well predicted (1987/1988, 1994/1995, and 1997/1998).

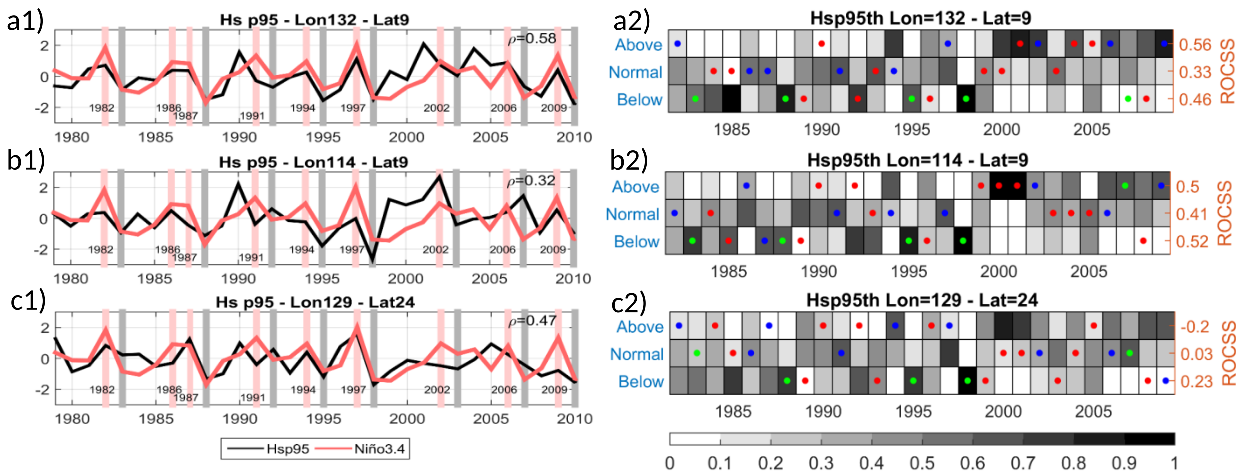

Figure 6. Detail of forecast skill for the following locations: a) [Lon=132.0°; Lat=9.0°]; b) [Lon=114.0°; Lat=9.0°]; and c) [Lon=129.0°; Lat=24.0°]. 1) Historical standardized time series of H_s observations and Niño 3.4 index. 2) Tercile validation plot of the 95th percentile of JJA Hs with terciles arranged by row. The number on the right shows the ROCSS for each tercile. Blue (green) dots mark the observed tercile during El Niño (La Niña) years. Red dots are the observed terciles for the rest of the years during the 1982-2009 period.

Figure 7 shows the ROCSS for the mean (upper panels) and the 95th percentile (lower panels) for the three categories: below-normal in the left column, normal in the middle column and above-normal in the right column. ROCSS scores of approximately 0.4-0.6 suggest skillful predictions for the lower and upper categories. The lack of skill for the normal category agrees with previous studies (Manzanas, 2016). The significant ROCSS indicates that forecasts in the highest probability bin have a greater hit rate than those in the lower probability bin, which can be observed in the above and below-normal categories in the tercile plot shown in panel a2 of Figure 6.

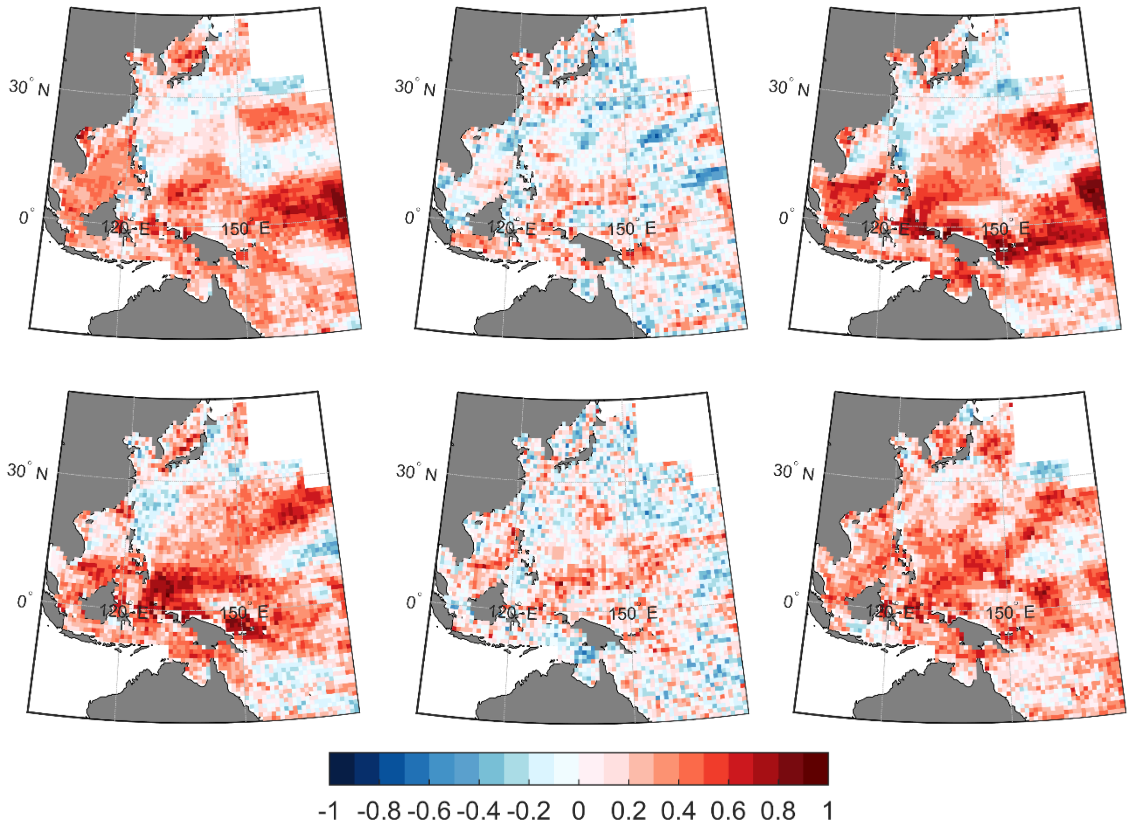

Figure 7. ROC Skill Score of the seasonal JJA wave height predictions in the Western Pacific Ocean (mean in the upper panels and 95th percentile in the lower panels) for the below normal, normal and above-normal terciles (left, middle and right column, respectively).

Figure 8 shows the maps of the ROCSS for El Niño events in the below-normal category. Negative anomalies are expected after the peak phase of NDJ ONI as a result of reduced atmospheric synoptic activity associated with an anomalous anticyclone that strengthens the West Pacific subtropical high (Lopez and Kirtman, 2016). An increase in the skill of these wave predictions is obtained, where the ROCSS is close to 1 over a wider area, and this result confirms that the warm phase of ENSO (El Niño events) is a source of skill for the JJA Hs anomalies (Lopez and Kirtman, 2016).

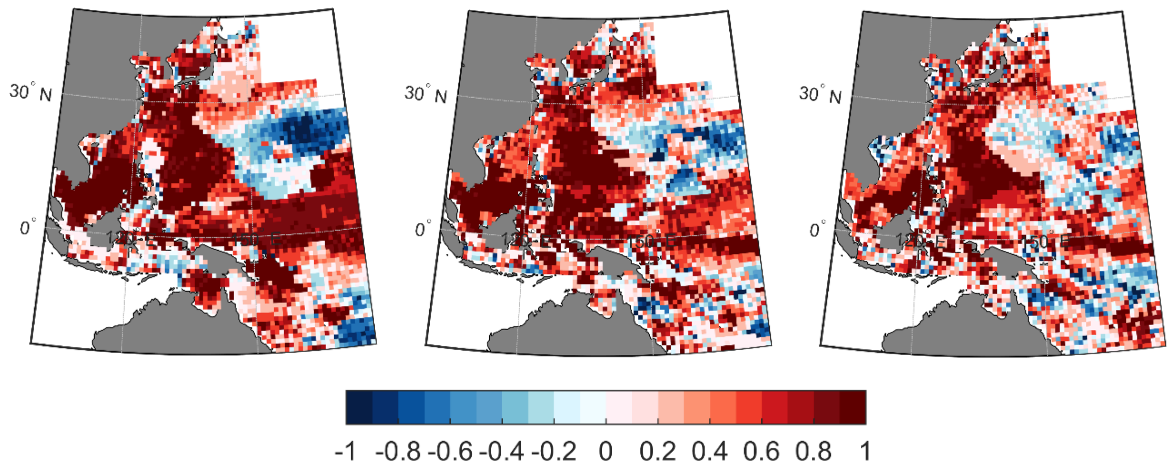

Figure 8. ROC Skill Score of the seasonal JJA wave height predictions in the Western Pacific Ocean (mean in the left panel, 95th percentile in the middle, and 99th percentile in the right panel) for the below-normal category.

4.2.2 North Atlantic

The correlation coefficient is shown in the left column of Figure 9 for the mean and 95th percentile of the JFM H_s. In general, correlation coefficients are smaller than 0.4 with an analogous spatial pattern for the different wave statistics. The bias (not shown) is negligible for the mean H_s and the 95th percentile, and the bias is slightly positive (<5%) for the 99th percentile. The forecast probability error, quantified by means of the RPS, is shown in the middle column of Figure 9. The RPS value is approximately 0.2-0.3, indicating a small probability error for the two wave height statistics. This finding could mean that the JFM forecast can discriminate among outcomes. However, the RPS strongly depends on the probability distribution among categories, which is lower when adjacent categories (e.g., normal and high) receive higher probabilities than when this occurs for the opposite categories (e.g., low and high). The analysis of the tercile plot in several locations along the North Atlantic Ocean (not shown) reveals that the ensemble mean predicted time series lies mostly in the *normal* category, with no category with a probability significantly larger than the rest. As a result, when above or below-normal categories occur, the opposite category is not predicted with high probability by the seasonal forecast, so the RPS is not penalized, which partially explains the obtained results. The RPSS is compared to the actual forecasts to the constant climatology forecasts. The RPSS is the opposite of RPS, where higher scores mean forecasts having higher skill levels. The RPSS is presented in the left panels of Figure 9. The values obtained are nonsignificant, ranging between -0.2 and 0.2 for almost the whole North Atlantic Ocean, except in the western part, where this verification score presents a higher negative value; this finding indicates an unsuccessful ability of the forecasts to differentiate among dissimilar observed outcomes compared to constant climatology forecasts (0.333/0.333/0.333). A similar forecast probability for all three categories is most likely to occur in the Western North Atlantic Ocean.

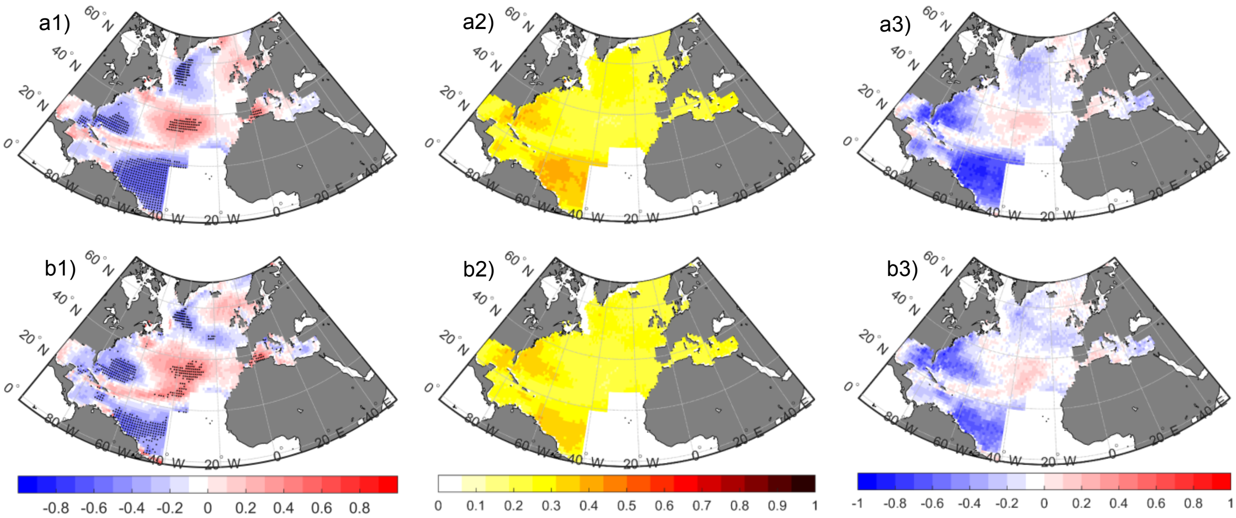

Figure 9. Verification of the JFM H_s: (a) mean and (b) 95th percentile in the North Atlantic Ocean using the 1) correlation coefficient; 2) RPS; and 3) RPSS.

ROCSS spatial maps of the JFM *H*s and SLP means are shown in Figure 10 for the below-normal, normal and above-normal categories (left, central and right columns, respectively). The area [40°W-20°W; 20°N-40°N] shows the highest predictability, especially for the lower tercile. Other locations in the North Sea and Western Mediterranean Sea also show high predictability. A similar ROCSS spatial distribution is obtained for the 95**th** percentile and nearly disappears for the 99**th** percentile (not shown). The ROCSS analysis of the JFM SLP predictions (input variable) shows a skillful area centered between the latitudes of 35°N and 55°N and the longitudes of 15°W and 55°W, which is reflected in the areas with higher JFM Hs prediction skill.

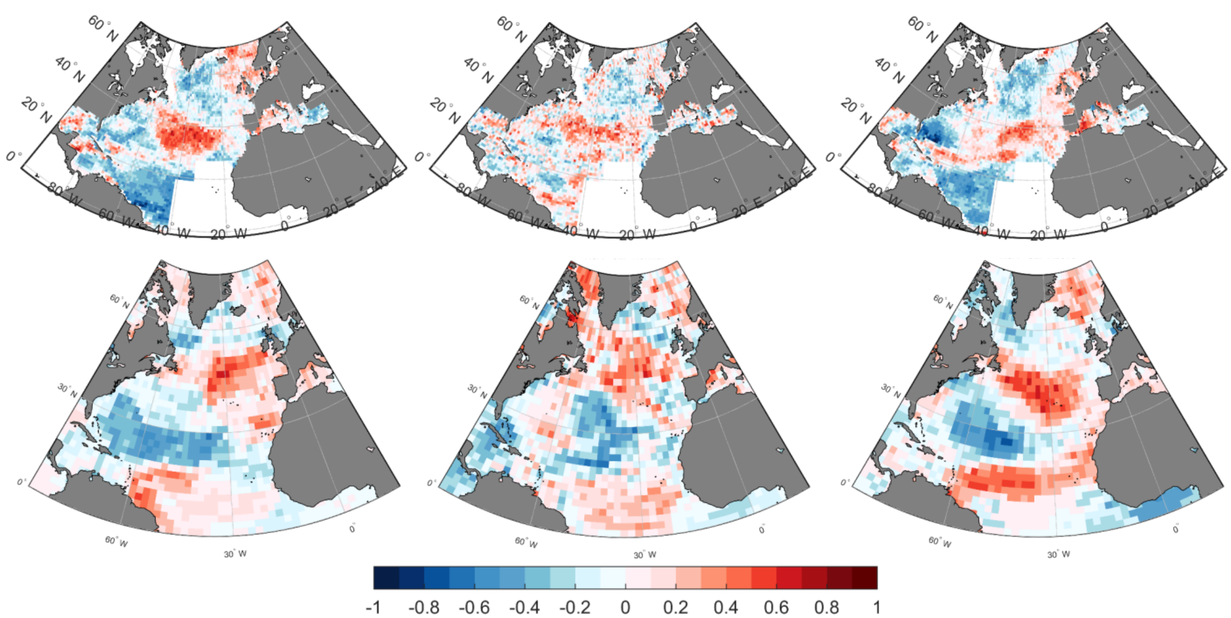

Figure 10. ROCSSs of the seasonal mean of JFM H_s predictions in the North Atlantic Ocean for the below normal, normal and above-normal terciles (left, central and right column, respectively) in the upper panels and of the mean winter sea level pressure fields in the lower panels.

5 Conclusions

The marine sector has not yet made use of climate services despite the broad range of potential applications in this sector, which includes but is not limited to seasonal forecasts. In this work, we have adapted the statistical downscaling framework proposed by Camus et al. 2017 for application to seasonal forecasting. The downscaled wave climate is obtained from the seasonal CFSv2 hindcast, which was analyzed and verified using the quasi-observational GOW2 wave database and a variety of deterministic and probabilistic metrics.

First, the suitability of a statistical downscaling approach to generate seasonal wave forecasts of the mean and 95th and 99th percentiles for the JJA season in the Western Pacific Ocean and for the JFM season in the Northern Atlantic Ocean were tested in perfect-prog conditions (i.e., using reanalysis data in the test period). With this aim, the quality of the NCEP-CFSv2 ensemble retrospective forecast (1982-2009) was assessed by validating the performance of the seasonal wave forecasting in the past, which was completed one month before the beginning of the validation period.

The statistical downscaling model in the Western Pacific shows a certain lack of skill due to differences in wave generation processes in this tropical area. This model configuration is considered to be as representative as possible of the main wave characteristics (swell component generated from distant storms that determinate the spatial domain of the predictor). The downscaled wave estimates in this region can be improved locally using particular predictors to represent wave generation from local winds or distant storms. Despite these limitations, downscaled seasonal JJA wave predictions in the Western Pacific show some predictability skill when assessed with the ROCSS probabilistic metric. The skill is higher during the decay years following the ENSO warm phases when a negative significant wave height anomaly is expected. Although years with large wave heights are related to ENSO because of the increase in TCs, a restricted performance of the statistical relationship is found. Scarce extreme events associated with TCs and the intrinsic limitations of the GCMs to reproduce the intensity of these atmospheric conditions lead to prediction failures in terms of detecting the positive wave height anomalies during these ENSO phases.

Statistical downscaling in the North Atlantic Ocean can capture the predictive signal in the global hindcast CFSR, but no relevant added value is found in terms of aggregating the predictability of the input atmospheric variable. The JFM wave forecast quality shows a similar performance to that of the SLP predictor. The low skill in this area is conditioned to the limited seasonal predictability over Europe in the retrospective database used. The skill pattern (evaluated by means of the ROCSS) of the seasonal wave forecast resembles the skill pattern of the seasonal SLP predictions. By applying the statistical downscaling model, the (low) predictor predictive skill is not lost.

Although the skill determined by the North Atlantic results was low to moderate (Kim et al., 2012), this experimental development opens the possibility of new applications to marine sectors. The new seasonal forecast system from the UK Met Office, GloSea5, has shown promising skill in predicting the NAO due to a considerable increase in resolution (Scaife et al., 2014). The emerging Copernicus Climate Change Service is expected to provide reliable and credible sources of free climate information in Europe in the coming years (EC, 2015), and therefore, this forecasting improvement combined with increased access to seasonal forecast data may lead to the application of these climate products within an operational framework in the near future.

The conclusions obtained in this work are only for summer wave heights in the Western Pacific and winter wave heights in the North Atlantic and may not be extended to other regions of the global ocean or seasons. Further investigation is still required to provide a more conclusive overview of the merits and limitations of statistical downscaled seasonal wave predictions.

Acknowledgments

P.C. acknowledges the support of the Spanish Ministerio de Economía y Competitividad (MINECO) and European Regional Development Fund (FEDER) under Grant BIA2015-70644-R (MINECO/FEDER, UE). The authors acknowledge funding from the ERANET ERA4CS (ECLISEA project) and the government of Cantabria and FEDER under the project CLISMO.

References

F. Ardhuin, E. Rogers, A.V. Babanin, J.-F. Filipot, R. Magne, A. Roland, A. Van der Westhuysen, P. Queffeulou, J.-M. Lefevre, L. Aouf, F. Collard. (2010). Semiempirical Dissipation source functions for ocean waves. Part I: definition, calibration, and validation, J. Phys. Oceanogr. 40 (9), 1917–1941.

Bedia, J., Golding, N., Casanueva, A., Iturbide, M., Buontempo, C., Gutiérrez, J.M. (2018). Seasonal predictions of Fire Weather Index: Paving the way for their operational applicability in Mediterranean Europe. Climate Services, 9, 101-110. https://doi.org/10.1016/j.cliser.2017.04.001.

Brands, S. (2017), Which ENSO teleconnections are robust to internal atmospheric variability?, Geophys. Res. Lett., 44, 1483–1493, doi:10.1002/2016GL071529.

Brands, S. (2014). Predicting average wintertime wind and wave conditions in the North Atlantic sector from Eurasian snow cover in October. Environmental Research Letters, 9 (4), art. no. 045006.

Bromirski, P. D., and Cayan, D. R. (2015), Wave power variability and trends across the North Atlantic influenced by decadal climate patterns, J. Geophys. Res. Oceans, 120, 3419–3443

Bruno Soares, M., Alexander, M., Dessai, S. (2018). Sectoral use of climate information in Europe: A synoptic overview. Climate Services, 9, 5-20. https://doi.org/10.1016/j.cliser.2017.06.001.

Camargo, S.J., Robertson, A.W., Gaffney, S.J., Smyth, P., Ghil, M. (2007). Cluster analysis of typhoon tracks. Part II: Large-scale circulation and ENSO, Journal of Climate, 20 (14), pp. 3654-3676.

Camus, P., Losada, I.J., Izaguirre, C., Espejo, A., Menéndez, M., Pérez, J. (2017). Statistical wave climate projections for coastal impact assessments. Earth's Future, 5 (9), pp. 918-933.

Casanueva, A. (2016). Comparison of statistical and dynamical climate downscaling techniques: screening of methods for their use in impact studies. . Ph.D. thesis, Universidad de Cantabria, 177 pp.

Castelle, B., Dodet, G., Masselink, G., Scott, T. (2017). A new climate index controlling winter wave activity along the Atlantic coast of Europe: The West Europe Pressure Anomaly Geophysical Research Letters, 44 (3), pp. 1384-1392.

Clark, R. T., P. E. Bett, H. E. Thornton, and A. A. Scaife (2017). Skillful seasonal predictions for the European energy industry. Environ. Res. Lett., 12, 024002, doi:10.1088/1748-9326/aa57ab.

Cohen, J. and Jones, J. (2011). A new index for more accurate winter predictions. Geophys. Res. Lett., 38, L21701.

Cofiño, A.S., Bedia, J., Iturbide, M., Vega, M., Herrera, S., Fernández, J., Frías, M.D., Manzanas, R., Gutiérrez, J.M. (2018). The ECOMS User Data Gateway: Towards seasonal forecast data provision and research reproducibility in the era of Climate Services. Climate Services, 9, 33-43. https://doi.org/10.1016/j.cliser.2017.07.001.

Colman, A. W., Palin, E. J., Sanderson, M. G., Harrison, R. T., Leggett, I. M. (2011). The potential for seasonal forecasting of winter wave heights in the northern North Sea. Weather Forecast, 26, 1067–74.

Doblas-Reyes, F.J., García-Serrano, J., Lienert, F., Biescas, A.P., Rodrigues, L.R.L. (2013). Seasonal climate predictability and forecasting: Status and prospects. Wiley Interdisciplinary Reviews: Climate Change, 4 (4), pp. 245-268.

Dodet, G., Bertin, X., Taborda, R. (2010). Wave climate variability in the North-East Atlantic Ocean over the last six decades, Ocean Modelling, 31, 120-131.

Dunstone, N., D. Smith, A. Scaife, L. Hermanson, R. Eade, N. Robinson, M. Andrews, and J. Knight (2016). Skilful predictions of the winter North Atlantic Oscillation one year ahead. Nat. Geosci., 9, 809–814, doi:10.1038/ngeo2824

European Commission, 2015: A European research and innovation Roadmap for Climate Services. [online] Luxembourg: European Commission. Available at: http://europa.eu/sinapse/webservices/dsp_export_attachement.cfm?CMTY_ID=0C46BEEC-C689-9F80-54C7DD45358D29FB&OBJECT_ID=552E851C-E1C6-AFE7-C9A99A92D4104F7E&DOC_ID=7805BB42-91F4-46A5-A8C87397412DBE00&type=CMTY_CAL.

Frías, M.D., M. Iturbide, R. Manzanas, J. Bedia, J. Fernández, S. Herrera, A.S. Cofiño, J.M. Gutiérrez (2018). An R package to visualize and communicate uncertainty in seasonal climate prediction, Environmental Modelling & Software, 99, 101-110.

Frías, M.D., Herrera, S., Cofiño, A.S., Gutiérrez, J.M. (2010). Assessing the skill of precipitation and temperature seasonal forecasts in Spain: Windows of opportunity related to ENSO events. Journal of Climate, 23 (2), 209-220.

Gutiérrez, J. M., D. San-Martín, S. Brands, R. Manzanas, and S. Herrera (2013). Reassessing Statistical Downscaling Techniques for Their Robust Application under Climate Change Conditions. Journal of Climate 26 (1): 171–188. https://doi.org/10.1175/JCLI-D-11-00687.1.

Hewitt, C., Buontempo, C., Newton, P. (2013). Using climate predictions to better serve society's needs. Eos, 94 (11), pp. 105-107.

Huang, B., Thorne, P.W., Banzon, V.F., Boyer, T., Chepurin, G., Lawrimore, J.H., Menne, M.J., Smith, T.M., Vose, R.S., Zhang, H.-M. (2017). Extended reconstructed Sea surface temperature, Version 5 (ERSSTv5): Upgrades, validations, and intercomparisons. Journal of Climate, 30(20), pp. 8179-8205.

Hurrell, J.W., (1995). Decadal trends in the North Atlantic Oscillation and relationships to regional temperature and precipitation. Science 269, 676-679.

Izaguirre, C., Méndez, F.J., Menéndez, M., Losada, I.J. (2011). Global extreme wave height variability based on satellite data. Geophysical Research Letters, 38 (10)

Jolliffe, I. T. and D. B. Stephenson (2003). Forecast verification: A practitioner's guide in atmospheric sciences. John Wiley & Sons.

Jones, P.D., Jonsson, T. and Wheeler, D. (1997). Extension to the North Atlantic Oscillation using early instrumental pressure observations from Gibraltar and South-West Iceland. Int. J. Climatol. 17, 1433-1450.

Kim, H.-M., Webster, P., and Curry, J. (2012). Seasonal prediction skill of ECMWF System 4 and NCEP CFSv2 retrospective forecast for the Northern Hemisphere winter, Clim. Dyn., 23, doi:10.1007/s00382-012-1364-6.

Kirtman, B., et al. (2014). The North American Multimodel Ensemble: Phase-1 seasonal-to-interannual prediction; phase-2 toward developing intraseasonal prediction. Bulletin of the American Meteorological Society, 95 (4), 585–601, doi:10.1175/BAMS-D-12-00050.1.

Kohavi, R. (1995). A Study of cross-validation and bootstrap for accuracy estimation and model selection, International Joint Conference on Artificial Intelligence, IJCAI.

Lopez, H., and B. P. Kirtman (2016), Investigating the seasonal predictability of significant wave height in the West Pacific and Indian Oceans, Geophys. Res. Lett., 43, 3451–3458, doi:10.1002/2016GL068653.

Manzanas, R. (2016). Statistical downscaling of precipitation in seasonal forecasting: Advantages and limitations of different approaches. Ph.D. thesis, Universidad de Cantabria, 200 pp., URL http://meteo.unican.es/en/node/73340

Manzanas, R., Gutiérrez, J.M., Fernández, J., van Meijgaard, E., Calmanti, S., Magariño, M.E., Cofiño, A.S., Herrera, S. (2018a). Dynamical and statistical downscaling of seasonal temperature forecasts in Europe: Added value for user applications. Climate Services, 9, 44-56.

Manzanas, R., A. Lucero, A. Weisheimer, and J. M. Gutiérrez (2018b). Can Bias Correction and Statistical Downscaling Methods Improve the Skill of Seasonal Precipitation Forecasts?. Climate Dynamics 50 (3–4): 1161–76. https://doi.org/10.1007/s00382-017-3668-z.

Nikulin, G., Asharaf, S., Magariño, M.E., Calmanti, S., Cardoso, R.M., Bhend, J., Fernández, J., Frías, M.D., Fröhlich, K., Früh, B., García, S.H., Manzanas, R., Gutiérrez, J.M., Hansson, U., Kolax, M., Liniger, M.A., Soares, P.M.M., Spirig, C., Tome, R., Wyser, K. (2018). Dynamical and statistical downscaling of a global seasonal hindcast in eastern Africa Climate Services, 9, 72-85.

Perez, J., M. Menendez and I.J. Losada (2017), GOW2: A global wave hindcast for coastal applications, Coastal Engineering, Volume 124, Pages 1-11, doi:10.1016/j.coastaleng.2017.03.005.

Saha, S., S. Moorthi, X. Wu, J. Wang, S. Nadiga, P. Tripp, D. Behringer, Y.T. Hou, H.Y. Chuang, M. Iredell, M. Ek, J. Meng, R. Yang, M.P.n. Mendez, H. van den Dool, Q. Zhang, W. Wang, M. Chen and E. Becker (2014), The NCEP Climate Forecast System Version 2. Journal of Climate 27, 2185-2208, doi: 10.1175/JCLI-D-12-00823.1.

Saha, S., Moorthi, S., Wu, X., Wang, J., Nadiga, S., Tripp, P., Behringer, D., Hou, Y.T., ya Chuang, H., Iredell, M., Ek, M., Meng, J., Yang, R., Mendez, M.P., van den Dool, H., Zhang, Q., Wang, W., Chen, M., Becker, E. (2011). NCEP climate forecast system version 2 (cfsv2) 6-hourly products. URL:https://doi.org/10.5065/D61C1TXF.

Semedo, A., Sušelj, K., Rutgersson, A., Sterl, A. (2011). A global view on the wind sea and swell climate and variability from ERA-40. Journal of Climate, 24 (5), pp. 1461-1479.

Shukla, R.P., Kinter, J.L. Subseasonal prediction of significant wave heights over the western pacific and Indian ocean region (2016). Weather and Forecasting, 31 (6), pp. 1733-1751.

Scaife, A. A., et al. (2014), Skillful long-range prediction of European and North American winters, Geophys. Res. Lett., 41, 2514–2519, doi:10.1002/2014GL059637.

Stopa, J. E., and K. F. Cheung (2014). Periodicity and patterns of ocean wind and wave climate, J. Geophys. Res. Oceans, 119, 5563–5584, doi:10.1002/2013JC009729.

Stopa, J.E., Cheung, K.F., Tolman, H.L., Chawla, A. (2012). Patterns and cycles in the climate forecast system reanalysis wind and wave data. Ocean Modell, http://dx.doi.org/10.1016/j.ocemod.2012.10.005

Timmermans, B., D. Stone, M. Wehner, and H. Krishnan (2017). Impact of tropical cyclones on modeled extreme wind-wave climate. Geophysical Research Letters, 44, pp. 1393–1401.

Tolman, H. and theWaveWatch III® Development Group (2014), User Manual and System Documentation of WAVEWATCH III® version 4.18. Tech. Note 316, NOAA/NWS/NCEP/MMAB, 282 pp. +Appendices. https://doi.org/10.1021/ic501637m.

Torralba, V., Doblas-Reyes, F.J., MacLeod, D., Christel, I., Davis, M. (2017). Seasonal climate prediction: A new source of information for the management of wind energy resources. Journal of Applied Meteorology and Climatology, 56 (5), pp. 1231-1247.

Trigo, R.M., Valente, M.A., Trigo, I.F., Miranda, P.M.A., Ramos, A.M., Paredes, D., García-Herrera, R. (2008). The impact of North Atlantic wind and cyclone trends on European precipitation and significant wave height in the Atlantic. Annals of the New York Academy of Sciences, 1146, pp. 212-234.

Wang, X. L., Y. Feng, and V. R. Swail (2014). Changes in global ocean wave heights as projected using multi model CMIP5 simulations, Geophys. Res. Lett., 41(3), 1026–1034. https://doi.org/10.1002/2013GL058650.

Woolf, D.K., Challenor, P.G., Cotton, P.D. (2002). Variability and predictability of the North Atlantic wave climate Journal of Geophysical Research C: Oceans, 107 (10), pp. 9-1.

Yun, K. S., K. J. Ha, S. W. Yeh, B. Wang, and B. Xiang (2015). Critical role of boreal summer North Pacific subtropical highs in ENSO transition, Clim. Dyn., 44(7–8), 1979–1992.